The three-dimensional rotation neural network

J.W. Shuai*, J.C. Zheng, Z.X. Chen, R.T. Liu, B.X. Wu

Physics Department, Xiamen University, Xiamen 361005, PR China

Abstract

The storage capacity of the three-dimensional rotation neural network model is discussed by using the signal-to-noise theory. Some results discussed in the Hopfield model, the complex phasor model and the Hamilton neural network are obtained. Compared to other multistate neural networks, a novel property of the model is that the storage capacity for a fixed neuronal state varies with the different combinations of numbers of rotation angles and axes. The maximum storage capacity can be obtained for a special combination of numbers of rotation angles and axes.

1. Introduction

In recent years, growing interest has been focused on the multistate neural network models in order to process the multistate gray or color patterns. A complex state such as a color or gray pixel in the pattern can be expressed by a multistate neuron with these schemes. Variant neural networks can aid the emerging technology of neurocomputing by suggesting or analyzing new design schemes. Viewed from biology, these schemes perhaps are more realistic and may be helpful for understanding some of the basic aspects of biological information processing.

Kanter proposed a model composed of Potts neurons with Q possible discrete states [1]. Rieger used neurons represented by Q real numbers [2]. Another possibility for a multistate neuron is the so-called circular representation, in which the state of the neuron is represented by points on the circle. One is the complex phasor model proposed by Noest [3] and the other is the clock model proposed by Cook [4]. The complex phasor model and the clock model can be regarded as an extension of the Hopfield model [5] to the clock-type ones. The layered phasor neural networks [6] are discussed by Bolle. By introducing the 2^n-element numbers to the network, we discussed the

---

* Corresponding author. E-mail: jwshuai@cityu.edu.hk.

2^n-element number neural model [7,8]. Actually, the four-state complex neural network [9] discussed by Zhou is a special case of the complex phasor model and the 2^n-element number model. Nakamura considers a general extension of the Hopfield model using D-dimensional spins (i.e. D-dimensional unit vectors) as neurons [10].

In the view of the rotation, the bipolar (± 1) Hopfield model [5] is the one-dimensional rotation neural network model. The complex phasor neural network model [3] is the two-dimensional rotation neural network model. Along the lines of rotation, the D-dimensional rotation neural networks can be set up naturally. In this paper, the multistate three-dimensional rotation neural network model is discussed, in which the three-dimensional rotation operator is the state of the neuron. Many discussed neural models are the special cases of the present model, such as the bipolar Hopfield model [5], the four-state complex neural model [8,9], the complex phasor model [3] and the sixteen-state Hamilton neural model [7,8]. Compared to other multistate neural networks, the model allows various combinations of states of rotation angles and axes for a fixed neuron state. Therefore, a novel property of the model is that the storage capacity for a fixed neuronal state Q varies with the different combinations of states of rotation angles and axes, and there is a maximum storage capacity for a special combination of numbers of rotation angles and axes. In view of application, the advantage of the model is that it is especially appropriate for recognizing the color patterns that are composed of three basic colors widely used in computers.

The paper is organized as follows: In Section 2, the general framework of the three-dimensional rotation neural network is discussed. After introducing adiabatic-like approximation to the model in Section 3, the following two sections are devoted to analyze the correctly iterating probabilities of the rotation angle and axis. Then the storage capacity of the model is discussed in Section 6. Finally, the conclusion and application are discussed.

2. The three-dimensional rotation neural network

We know that the rotation operator $R(n, \theta_0)$ in a three-dimensional space, with its rotation axis $n = (i \cos \theta_1 + j \cos \theta_2 + k \cos \theta_3)$ and rotation angle θ_0 around the axis n, can be expressed as follows:

$$R(n, \theta_0) = \cos \theta_0 + \sin \theta_0 (i \cos \theta_1 + j \cos \theta_2 + k \cos \theta_3). \tag{1}$$

Here, i, j, k are the three basic vectors of the coordinate axes, the rotation angle $0 \leqslant \theta_0 < 2\pi$ and the direction angles $0 \leqslant \theta_1, \theta_2 < \pi, -\pi/2 \leqslant \theta_3 < \pi/2$. The conjugate rotation of $R(n, \theta_0)$ is $R^*(n, \theta_0) = R(n, 2\pi - \theta_0)$ and we have $(R_1 R_2)^* = R_2^* R_1^*$. It should be noted that normally $R_1 R_2 \neq R_2 R_1$.

By introducing the concept of three-dimensional rotation into the neural network, the multistate discrete three-dimensional rotation model can be set up. The state of a
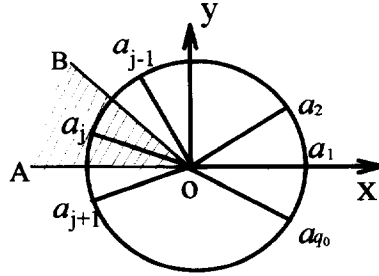
Fig. 1. Sketch map of the values of rotation angle and its mapping area.

neuron is defined as a rotation operator and can be expressed as follows:

$$S = R(\boldsymbol{m}_i, \alpha_j) = R(\boldsymbol{i}\cos\beta_{1i} + \boldsymbol{j}\cos\beta_{2i} + \boldsymbol{k}\cos\beta_{3i}, \alpha_j). \tag{2}$$

Here $i = 1, 2, \ldots, q_1$ and $j = 1, 2, \ldots, q_0$. It means that there are q_1 discrete axes $\boldsymbol{m}_i$ with the direction angles $\beta_{1i}, \beta_{2i}, \beta_{3i}$ and q_0 discrete rotation angles α_j around the axes for the neuron states. So there are $Q = q_0 q_1$ discrete neuron states for the three-dimensional rotation model. Normally, we can let the distribution of the axes and rotation angles be homogeneous. Fig. 1 shows the q_0 rotation angles $(\alpha_1, \alpha_2, \ldots, \alpha_j, \ldots, \alpha_{q_0}) = (0, 2\pi/q_0, \ldots, 2(j-1)\pi/q_0, \ldots, 2(q_0-1)\pi/q_0)$ that homogeneously distribute on the 2π rotational plane.

Suppose there are N neurons and M patterns $S^\mu = (S_1^\mu, S_2^\mu, \ldots, S_N^\mu)$ in which $\mu = 1, 2, \ldots, M$ stored in the network. The synaptic connection matrix is given by the Hebbian learning rule:

$$J_{ij} = \sum_{\mu=1}^{M} S_i^\mu (S_j^\mu)^*. \tag{3}$$

One can easily see that $J_{ij}^* = J_{ji}$. If a pattern $S(t)$ is put into the network, the iterating dynamics of the model depends on the effective local field H,

$$H_i(t) = \sum_{j=1}^{N} J_{ij} S_j(t). \tag{4}$$

Actually, the effective local field H_i is the total rotation operator, but is commonly not the normalized rotation operator,

$$H_i(t) = |H_i(t)| R(\boldsymbol{n}_i(t), \theta_{0i}(t)). \tag{5}$$

The energy function $E(S)$ can also be defined for the state S with the interacting J:

$$E(S) = -\frac{1}{2N^2} \sum_{i=1}^{N} \sum_{j=1}^{N} S_i^* J_{ij} S_j. \tag{6}$$

The energy function is an extension of that of the bipolar Hopfield model [5], the complex phasor model [11,12] and the Hamilton neural model [13].

The nonlinear iterating dynamics of the network from $S(t)$ to $S(t+1)$ is defined as follows:

$$R_i(m_k(t+1), \alpha_j(t+1)) = \Theta(H_i(t)) = \Theta(R(n_i(t), \theta_{0i}(t))) . \tag{7}$$

For the discrete model, the mapping rule of the transform function Θ is usually defined as that it maps a range of rotation operators to one of the discrete neuronal rotation states. To the rotation angle, because the q_0 discrete neuronal rotation angles are homogeneously distributed on the 2π circle plane, the rotation angle θ_{0i} of the local field is mapped by the function Θ to its nearest neuronal rotation angle α_j. As shown in Fig. 1, there are q_0 sectors that consist of q_0 bisectors of the q_0 neuronal state pixels. Any rotation angle in a specific sector is mapped by Θ to the neuronal rotation angle expressed by the central pixel. For example, if $-\pi/q_0 \leqslant \theta_{0i} < \pi/q_0$, it is mapped to $\alpha_0 = 0$; if $(2j-3)\pi/q_0 \leqslant \theta_{0i} < (2j-1)\pi/q_0$, it is mapped to $\alpha_j = 2(j-1)\pi/q_0$. To the direction angle, there are q_1 neuronal rotation axes, and all the axes in the $2\pi/q_1$ solid angle around each neuronal axis is mapped by Θ to that neuronal axis.

If we let $q_1 = 1$ and $m = i$, the state of the neuron is

$$S = \cos\alpha_j + i\sin\alpha_j = \exp(i\alpha_j) . \tag{8}$$

Actually, it is the complex phasor neural network [3,12]. Furthermore, if defining $q_0 = 2$ and $\alpha_1 = 0, \alpha_2 = \pi$, the states of the neuron are $S = \pm 1$ and it becomes the Hopfield model [5]. Or if defining $q_0 = 4$, and $\alpha = \pm\pi/4, \pm3\pi/4$, the states of the neuron are $S = (\pm 1 \pm i)/\sqrt{2}$ that goes to the four-state complex model [8,9].

If we define the centerlines of eight quadrants as the rotation axes m of the neuron states and $q_0 = 2$ with the rotation angles α_1, α_2 in which $\sin\alpha_1 = \sqrt{3}/4, \cos\alpha_1 = \frac{1}{4}$ and $\alpha_2 = \pi + \alpha_1$, the neuron is of sixteen states: $(\pm 1 \pm i \pm j \pm k)/4$. Simply we can let the neuron states be $(\pm 1 \pm i \pm j \pm k)$. The iterating dynamics (7) can be defined as: each axis in a specific quadrant is mapped to its centerline; the rotation angle θ_0 is mapped to α_1 if $-\pi/2 < \theta_0 \leqslant \pi/2$, otherwise to α_2. Then there is a simple expression for the iterating dynamics: whenever a real or imaginary component of H is nonnegative, a positive unit is drawn out for the corresponding component of ΘH; otherwise, a negative unit drawn out. Therefore, the sixteen-state Hamilton neural network [7,8] is obtained. From the view of the 2^n-element numbers, the complex phasor model [3,11,12] is an extension of the four-state complex neural network [8,9]. Similarly, the three-dimensional model is an extension of the sixteen-state Hamilton number neural network.

3. The adiabatic-like approximation

To analyse the storage capacity of the model, i.e. $\Gamma = M/N$, let the number of neurons N and the number of stored patterns M approach infinity. At first the adiabatic-like approximation is discussed in this section. If the pattern $S^{\mu=1}$ is put into the

network, the effective local fields H_i can be expanded as follows:

$$H_{0i} = N \cos \alpha_i^1 + \Delta_{0i} ,\tag{9}$$

$$H_{1i} = N \sin \alpha_i^1 \cos \beta_{1i}^1 + \Delta_{1i} ,\tag{10}$$

$$H_{2i} = N \sin \alpha_i^1 \cos \beta_{2i}^1 + \Delta_{2i} ,\tag{11}$$

$$H_{3i} = N \sin \alpha_i^1 \cos \beta_{3i}^1 + \Delta_{3i} ,\tag{12}$$

where α_i^1 and β_{mi}^1 ($m = 1, 2, 3$) are the rotation angle and the direction angles of the ith neuron in the first stored pattern, respectively. Clearly, in the expanded expressions Eqs. (9)–(12), the local fields are divided into two parts: the first terms are the signals while the second terms the noises. The expressions for the noise terms Δ_{0i} and Δ_{mi} can be written out respectively. For example, the noise term of the rotation angle part is expressed as follows:

$$\begin{aligned}
\Delta_{0i} = \sum_{\mu=2}^{M} \sum_{j=1}^{N} &[\cos \alpha_i^\mu (\cos \alpha_j^\mu \cos \alpha_j^1 + \sin \alpha_j^\mu \cos \beta_{1j}^\mu \sin \alpha_j^1 \cos \beta_{1j}^1 \\
&+ \sin \alpha_j^\mu \cos \beta_{2j}^\mu \sin \alpha_j^1 \cos \beta_{2j}^1 + \sin \alpha_j^\mu \cos \beta_{3j}^\mu \sin \alpha_j^1 \cos \beta_{3j}^1) \\
&+ \sin \alpha_i^\mu \cos \beta_{1i}^\mu (\sin \alpha_j^\mu \cos \beta_{1j}^\mu \cos \alpha_j^1 - \cos \alpha_j^\mu \sin \alpha_j^1 \cos \beta_{1j}^1 \\
&+ \sin \alpha_j^\mu \cos \beta_{2j}^\mu \sin \alpha_j^1 \cos \beta_{3j}^1 - \sin \alpha_j^\mu \cos \beta_{3j}^\mu \sin \alpha_j^1 \cos \beta_{2j}^1) \\
&+ \sin \alpha_i^\mu \cos \beta_{2i}^\mu (\sin \alpha_j^\mu \cos \beta_{2j}^\mu \cos \alpha_j^1 - \cos \alpha_j^\mu \sin \alpha_j^1 \cos \beta_{2j}^1 \\
&+ \sin \alpha_j^\mu \cos \beta_{3j}^\mu \sin \alpha_j^1 \cos \beta_{1j}^1 - \sin \alpha_j^\mu \cos \beta_{1j}^\mu \sin \alpha_j^1 \cos \beta_{3j}^1) \\
&+ \sin \alpha_i^\mu \cos \beta_{3i}^\mu (\sin \alpha_j^\mu \cos \beta_{3j}^\mu \cos \alpha_j^1 - \cos \alpha_j^\mu \sin \alpha_j^1 \cos \beta_{3j}^1 \\
&+ \sin \alpha_j^\mu \cos \beta_{1j}^\mu \sin \alpha_j^1 \cos \beta_{2j}^1 - \sin \alpha_j^\mu \cos \beta_{2j}^\mu \sin \alpha_j^1 \cos \beta_{1j}^1)] .
\end{aligned}\tag{13}$$

Owing to the random character of the stored patterns and their independence to each other, it is reasonable to suppose that the noise terms are governed by a Gaussian distribution

$$g(x) = \frac{1}{\sqrt{2\pi}\sigma} \exp \left(-\frac{x^2}{2\sigma^2} \right) ,\tag{14}$$

with expectation value $\langle \Delta_{0i} \rangle = \langle \Delta_{mi} \rangle = 0$ and standard deviation

$$\sigma = \langle \Delta_{0i}^2 \rangle^{1/2} = \langle \Delta_{mi}^2 \rangle^{1/2} = \sqrt{N(M-1)/2} .$$

Here $\langle \rangle$ indicates the average of the stored patterns.

Using the signal-to-noise theory to analyze the storage capacity Γ, the crux is to obtain the probability ρ that the local field can be correctly iterated with the dynamics equation (7), i.e. to solve the probability of

$$\Theta(H_i) = R(\boldsymbol{m}_i^1, \alpha_i^1) = R(\boldsymbol{i} \cos \beta_{1i}^1 + \boldsymbol{j} \cos \beta_{2i}^1 + \boldsymbol{k} \cos \beta_{3i}^1, \alpha_i^1) .\tag{15}$$

Because of the coupling of the direction angles and the rotation angle, it is difficult to analyze Eqs. (9)–(12) directly. But we can rewrite them as Eqs. (18) and (25) correctly if the local field can be correctly iterated. Thus we introduce the adiabatic-like approximation: The coupling of the direction angles and the rotation angle can be ignored with statistical average. It means that when we deal with one kind of angle, the other is taken as a constant with its statistical average. Then the local field can be divided into two parts:

(A) For the rotation angle, due to the approximation, we take the direction angles as constants. Then one can easily combine Eqs. (10)–(12) as Eq. (17) and have

$$H_{0i}^R = N \cos \alpha_i^1 + \Delta_{0i}^R \,, \tag{16}$$

$$H_{0i}^I = N \sin \alpha_i^1 + \Delta_{0i}^I \,. \tag{17}$$

The above two equations can be rewritten in the form of a complex:

$$\tilde{H}_{0i} = N \exp(i\alpha_i^1) + \Delta_0 \exp(i\omega) \,. \tag{18}$$

Here, N is the weight that the rotation angle α_i^1 can be correctly iterated. For the noise term, i.e. the second term, the modulus $\Delta_0 = \sqrt{\Delta_{0i}^R + \Delta_{0i}^I}$ is governed by the positive Gaussian distribution

$$f(r) = 2g(r) = \sqrt{\frac{2}{\pi\sigma_0}} \exp\left(-\frac{x^2}{2\sigma_0^2}\right) \tag{19}$$

with $\int_0^\infty f(r)\,dr = 1$, with average zero and standard deviation

$$\sigma_0 = \langle \Delta_{0i}^R \rangle^{1/2} + \langle \Delta_{0i}^I \rangle^{1/2} = \sqrt{N(M-1)} \tag{20}$$

and the phasor ω is homogeneously distributed over the range $(0, 2\pi)$, owing to the symmetrization of Δ_{0i}^R and Δ_{0i}^I.

(B) For the direction angles, i.e. the rotation axis, due to the adiabatic-like approximation, the rotation angle α_i^1 is taken as a constant and $\sin \alpha_i^1$ is replaced by its standard deviation

$$\eta = \langle \sin^2 \alpha_i^1 \rangle^{1/2} = \frac{\sqrt{2}}{2} \,. \tag{21}$$

Then

$$H_{1i} = \eta N \cos \beta_{1i}^1 + \Delta_{1i} \,, \tag{22}$$

$$H_{2i} = \eta N \cos \beta_{2i}^1 + \Delta_{2i} \,, \tag{23}$$

$$H_{3i} = \eta N \cos \beta_{3i}^1 + \Delta_{3i} \,. \tag{24}$$

And expressed as a three dimensional vector

$$\boldsymbol{H}_i = \eta N \boldsymbol{m}_i^1 + \boldsymbol{\Delta}_i \,. \tag{25}$$
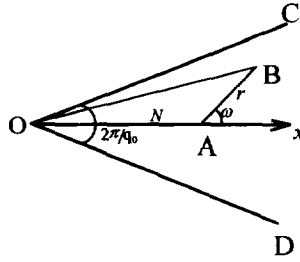
Fig. 2. The complex plane geometric interpretation of iterating dynamics of rotation angle.

Here ηN is the weight that the rotation axis $\boldsymbol{m}_i^1 = (\boldsymbol{i}\cos\beta_{1i}^1 + \boldsymbol{j}\cos\beta_{2i}^1 + \boldsymbol{k}\cos\beta_{3i}^1)$ can be correctly iterated, and $\boldsymbol{\Delta}_i = \Delta_{1i}\boldsymbol{i} + \Delta_{2i}\boldsymbol{j} + \Delta_{3i}\boldsymbol{k}$ is the noise term. Also, the modulus $|\Delta_i|$ is governed by the positive Gaussian distribution (19) with average zero and standard deviation

$$\sigma_1 = \langle\Delta_{1i}^2\rangle^{1/2} + \langle\Delta_{2i}^2\rangle^{1/2} + \langle\Delta_{3i}^2\rangle^{1/2} = \sqrt{3N(M-1)/2} \tag{26}$$

and the direction of Δ is homogeneously distributed on the 4π solid angle, i.e. sphero-symmetry.

After introducing adiabatic-like approximation, the probability ρ that the local field of the ith neuron can be correctly iterated with the dynamics equation (7) equals the product of the correctly iterating probabilities of rotation angle (18) and the rotation axis (25). In the following two sections, the correctly iterating probabilities of the rotation angle and the rotation axis are analyzed, respectively.

4. The correctly iterating probability of the rotation angle

The correctly iterating probability of the rotation angle is determined by Eq. (18). Because the model is symmetric under the rotation operator, without loss of generality, assume that the rotation angle $\alpha_i^1 = 0$, then

$$\tilde{H}_{0i} = N + \Delta_0 \exp(i\omega) = |H_{0i}|\exp(i\phi_i). \tag{27}$$

According to the dynamical equation (7), the condition that the rotation angle α_i^1 can be iterated correctly is $-\pi/q_0 \leqslant \phi_i < \pi/q_0$. Based on the view of geometry, which is shown in Fig. 2, N is expressed as the vector OA on the real axis, and the noise term $\Delta_0 \exp(i\omega)$ is expressed as the vector AB. The length of the vector AB follows a Gaussian distribution, and the angle $\angle x$AB is ω. Then $\tilde{H}_{0i}$ is the sum of the vectors OA and AB, i.e. OB = OA + AB. Accordingly, the condition $-\pi/q_0 \leqslant \phi_i < \pi/q_0$ means that $-\pi/q_0 \leqslant \angle$ AOB $< \pi/q_0$, i.e. point B must fall into the sector COD.
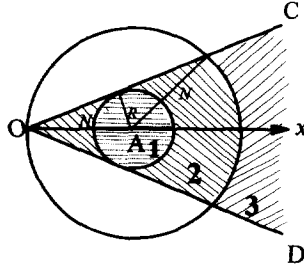
Fig. 3. The sketch map of the integration equation (28).

So the probability ρ_1 that the rotation angle is able to iterate correctly equals the probability that point B falls in the sector COD, and is then expressed as

$$\rho_1 = \int\limits_0^{r_0} f(r)\,dr + \int\limits_{r_0}^{N} \left(1 - \frac{2}{\pi}\arccos\frac{r_0}{r}\right) f(r)\,dr$$

$$+ \int\limits_N^{\infty} \left(1 - \frac{1}{\pi}\arccos\frac{r_0}{N} - \frac{1}{\pi}\arccos\frac{r_0}{r}\right) f(r)\,dr. \tag{28}$$

Here, $r_0 = N\sin(\pi/q_0)$ is the radius of the circle with center at A and tangent to the sector $\angle COD$, as shown in Fig. 3 and shaded with dotted lines. The probability is expressed as the integration of the weighted Gaussian function $f(r)$, in which the weight coefficient indicates the proportion of the sector COD compared to the whole circle in the corresponding distance r. The first term is expressed as the probability that point B falls in the circular area 1 that is shown in Fig. 3. The second term is expressed as the probability that the point B falls in the area 2 shaded with inverse-oblique lines shown in Fig. 3, consisting of the intersection of the sector COD and the circular band with center at point A, inner radius r_0, and outer radius N. The third term is expressed as the probability that the point B falls in the area 3 shaded with oblique lines shown in Fig. 3, consisting of the intersection of the sector COD and the circular band area with center at point A, inner radius N, and outer radius ∞.

The probability ρ_1 can be rewritten as the follows:

$$\rho_1 = 1 - \int\limits_{r_0}^{N} \frac{2}{\pi}\arccos\left(\frac{r_0}{r}\right) f(r)\,dr$$

$$- \int\limits_N^{\infty} \frac{1}{\pi}\arccos\left(\frac{r_0}{N}\right) f(r)\,dr - \int\limits_N^{\infty} \frac{1}{\pi}\arccos\left(\frac{r_0}{r}\right) f(r)\,dr. \tag{29}$$

If N is very large, one can write

$$\int\limits_{N}^{\infty} \arccos\left(\frac{r_0}{N}\right) f(r)\, dr \approx \int\limits_{N}^{\infty} \arccos\left(\frac{r_0}{r}\right) f(r)\, dr \,. \tag{30}$$

And when r varies from r_0 to ∞, $\arccos(r_0/r)$ varies from 0 to $\pi/2$; and the computer numerical simulation result indicates that the change of ρ_1 with r_0 mainly depends on the change of the function $f(r)$ with r_0. So the function $\arccos(r_0/r)$ can be replaced by a constant coefficient A with $0 < A < \pi/2$ and moved outside the definite integral [14]. Therefore, the expression for the probability ρ_1 can be approximated by

$$\rho_1 \approx 1 - \frac{2A}{\pi} \int\limits_{r_0}^{\infty} f(r)\, dr$$

$$\approx 1 - \frac{2A}{\pi} \left[1 - \sqrt{1 - \exp\left(-\frac{r_0^2}{2\sigma_0^2}\right)} \right]$$

$$\approx 1 - \frac{2A}{\pi} \left[1 - \sqrt{1 - \exp\left(-\frac{1}{2\Gamma} \sin^2 \frac{\pi}{q_0}\right)} \right]. \tag{31}$$

5. The correctly iterating probability of the rotation axis

The correctly iterating probability of the direction angles is determined by Eq. (25). As in the above section, without loss of generality, assume that the rotation axis $m_i^1 = k$, then Eq. (25) is

$$H_i = \eta N k + \Delta_i \,. \tag{32}$$

Based on the view of solid geometry, which is shown in Fig. 4, $\eta N k$ is expressed as the vector OE on the k-axis, and the noise term Δ_i as the vector EF. The length of the vector EF follows the Gaussian distribution (19), and the direction sphero-symmetry. Then H_i is the vectors $OF = OE + EF$. Now, according to solid geometry, the condition that the rotation axis can be iterated correctly, i.e. $\Theta(H_i) = k$, is that the pixel F must fall into a special space with the $2\pi/q_1$ solid angle, in which the axis k is included. Without loss of generality, here let the space be a circular cone space OGH with the centerline k shown in Fig. 4.

Accordingly, the probability ρ_2 that the rotation axis can be iterated correctly equals to the probability that point F falls in the circular cone OGH. Similar to ρ_1, the probability ρ_2 is expressed as the integration of the weighted Gaussian function $f(r)$, and the weight coefficient indicates the proportion of the circular cone OGH compared
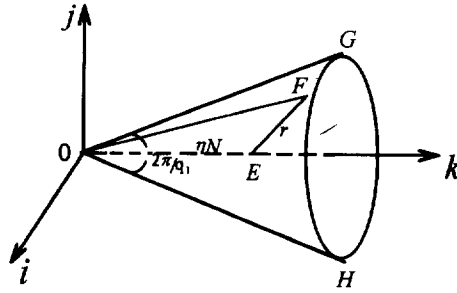
Fig. 4. The solid geometric interpretation of iterating dynamics of the rotation axis.

with the spherical space in the corresponding distance r, and can be expressed as

$$\rho_2 = \int_0^{R_0} f(r)\,\mathrm{d}r + \int_{R_0}^{\eta N} \frac{1}{2}(2 - \cos\varphi - \cos\phi)f(r)\,\mathrm{d}r$$

$$+ \int_{\eta N}^{\infty} \frac{1}{2}(1 - \cos\varphi)f(r)\,\mathrm{d}r\,, \tag{33}$$

in which $R_0 = \eta N/q_1\sqrt{2q_1 - 1}$ is the radius of the sphere I with center at E and tangent to circular cone OGH, as shown in Fig. 5 and the angles φ, ϕ are expressed as

$$\varphi = \psi + \arcsin\frac{R_0}{r}\,,$$

$$\phi = \arcsin\frac{R_0}{r} - \psi\,, \tag{34}$$

with

$$\psi = \arccos\left(1 - \frac{1}{q_0}\right)\,.$$

Here, the first term of Eq. (33) is expressed as the probability that point F falls in the spheroid space I shown in Fig. 5. The second term is expressed as the probability that the point F falls in the space II shaded with inverse-oblique lines shown in Fig. 5, consisting of the intersection of the circular cone OGH and the spheroid band with center at point E, inner radius R_0, and outer radius ηN. The third term is expressed as the probability that the point F falls in the space III shaded with oblique lines shown in Fig. 5, consisting of the intersection of the circular cone OGH and the spheroid band space with center at point E, inner radius ηN, and outer radius ∞.

Similar to the analysis of Eq. (30), the probability ρ_2 can be solved as

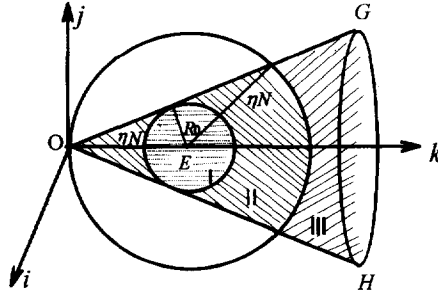$$\rho_2 = 1 - \int_{R_0}^{\eta N} \sqrt{1 - \frac{R_0^2}{r}}\cos\psi f(r)\,\mathrm{d}r$$

Fig. 5. The sketch map of the integration equation (33).

$$-\frac{1}{2}\int_{\eta N}^{\infty}\left(1+\sqrt{1-\frac{R_0^2}{r^2}}\cos\psi-\frac{R_0}{r}\sin\psi\right)f(r)\,\mathrm{d}r$$

$$\approx 1-\left(1-\frac{1}{q_1}\right)^2\left[1-\sqrt{1-\exp\left(-\frac{R_0^2}{2\sigma^2}\right)}\right]$$

$$=1-\left(1-\frac{1}{q_1}\right)^2\left[1-\sqrt{1-\exp\left(-\frac{2q_1-1}{6\Gamma q_1^2}\right)}\right].\tag{35}$$

6. The storage capacity of the model

From the results of the above two sections, the probability that the local field can be correctly iterated with the dynamics equation (7) can be obtained, i.e. $\rho = \rho_1\rho_2$. The erroneously iterating probability of the ith neuron is

$$P = 1-\rho$$

$$\approx \frac{2A}{\pi}\left[1-\sqrt{1-\exp\left(-\frac{1}{2\Gamma}\sin^2\frac{\pi}{q_0}\right)}\right]$$

$$+\left(1-\frac{1}{q_1}\right)^2\left[1-\sqrt{1-\exp\left(-\frac{2q_1-1}{6\Gamma q_1^2}\right)}\right]$$

$$\approx \frac{A}{\pi}\exp\left(-\frac{1}{2\Gamma}\sin^2\frac{\pi}{q_0}\right)+\frac{1}{2}\left(1-\frac{1}{q_1}\right)^2\exp\left(-\frac{2q_1-1}{6\Gamma q_1^2}\right).\tag{36}$$

Then on average, the number of erroneously iterating neurons for the input pattern S^1 is NP. To obtain the absolute storage capacity Γ_{abs} of the model that determines how many patterns are embedded as the equilibrium states of the network in the strict sense, we assume that the number of error components follows approximately the

Poisson distribution [15]. Therefore, the probability that S^1 is indeed a stable attractor is given approximately by the expression

$$\xi = \exp(-NP) \to 1 \,. \tag{37}$$

Now suppose we require that this probability be a fixed number very near 1; then inverting the preceding expression one can get $NP = C$, where $C = -\ln \xi$ is a constant approaching zero. This means that the number of erroneously iterating neurons is zero. Then the absolute storage capacity Γ_{abs} of the model is determined by

$$\frac{C}{N} = \frac{A}{\pi} \exp\left(-\frac{1}{2\Gamma_{abs}} \sin^2 \frac{\pi}{q_0}\right) + \frac{1}{2}\left(1 - \frac{1}{q_1}\right)^2 \exp\left(-\frac{2q_1 - 1}{6\Gamma_{abs} q_1^2}\right). \tag{38}$$

One can find the relationship between the absolute storage capacity and the number of neurons is shown as $\Gamma_{abs} \propto 1/\ln N$. This result holds true to its specific models: Hopfield model [15–17], four-state complex model [8,9], the Hamilton model [7,8] and the complex phasor model [14].

As mentioned above, the complex phasor model is the specific model of the three-dimensional rotation model only with $Q = q_1$ and $q_2 = 1$. For this case, the second term of Eq. (38) becomes zero and the absolute storage capacity can be written as

$$\Gamma_{abs} \propto \frac{1}{\ln N} \sin^2 \frac{\pi}{Q} \,. \tag{39}$$

It goes to the result that obtained in [14].

For the Hopfield model, the absolute storage capacity [15–17] determines how many patterns can be really stored in the network in the strict sense. However, the associative memory can work well when $\Gamma < \Gamma_{eff} \sim 0.14$ [18,19]. From analogy with spin glasses, one can imagine that there are many metastable states, which are separated by high energy barriers and exist around the memorized patterns, and that the retrieval close to the stored pattern becomes possible when Γ is smaller than the effective storage capacity Γ_{eff}. Similarly, to get the effective storage capacity of the three-dimensional rotation model, we let the number of erroneously iterating neurons $NP = \delta N$ in which the constant $\delta \to 0$, instead of $NP = C \to 0$. Then the effective storage capacity is determined by

$$\delta = \frac{A}{\pi} \exp\left(-\frac{1}{2\Gamma_{eff}} \sin^2 \frac{\pi}{q_0}\right) + \frac{1}{2}\left(1 - \frac{1}{q_1}\right)^2 \exp\left(-\frac{2q_1 - 1}{6\Gamma_{eff} q_1^2}\right). \tag{40}$$

Compared to the absolute storage capacity, the effective storage capacity is not dependent on the neuron number N.

For Eq. (40) with $q_0 = 2$ and $q_1 = 1$, i.e. the Hopfield model, $\Gamma_{eff} = -1/2 \ln(\delta\pi/A) \approx 0.144$ is obtained for $A = 1.0$ and $\delta = 0.009$. From Eqs. (38) and (40), one can see that the storage capacity decreases with the increase of $Q = q_0 q_1$, e.g. the storage capacity decreases from 0.144 to 0.03 and to 0.003 with the increase of (q_0, q_1) from
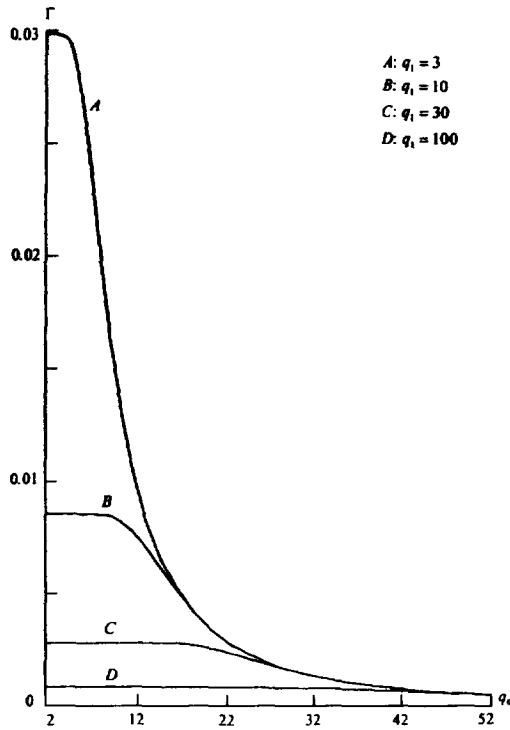
Fig. 6. The effective storage capacity Γ via q_0 with fixed $q_1 = 3, 10, 30$ and 100.

(2, 1) to (3, 3) and to (20, 20), and

$$\Gamma \to 0 \quad \text{with} \quad Q \to \infty.$$

To discuss in detail the dependence of the effective storage capacity Γ_{eff} with q_0 and q_1, we have plotted the solution of Eq. (40) for $A = 1.0$ and $\delta = 0.01$ in Figs. 6 and 7, respectively. We can interpret the result by considering the geometry shown in Figs. 3 and 5: as Q increases, the area of the sector COD and the volume of the circular cone OGH decrease, i.e. the probability that points B and F fall in the sector and cone decreases.

Here compared to other multistate neural networks, a novel property is shown for the model: With the fixed state number Q, the storage capacity varies with different combinations of q_0 and q_1. The computer numerical simulation is given in Fig. 8 with $Q = 15, 30, 50, 100$ and 500. With a fixed Q, there is a maximum storage capacity for a special combination of q_0 and q_1. In Fig. 8, the maximum storage capacity via Q is also given with dashed line. It should be pointed out that only the values with q_0 and q_1 integer are usable. We can interpret the result as follows. At the maximum point the distribution or the utilization of the iterating regions of the rotation angles and the axes of the neuron states is the best. On the other hand, at the two extremes with $q_0 = 2$, $q_1 = Q/2$ and $q_0 = Q$, $q_1 = 1$, the distribution of the iterating regions of the
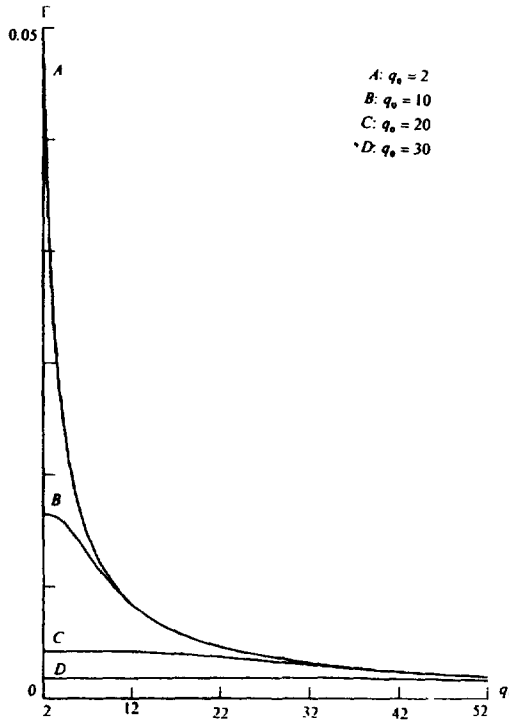
Fig. 7. The effective storage capacity Γ via q_1 with fixed $q_0 = 2, 10, 20$ and 30.

neuron states for the iterating dynamical Eq. (7) is extremely unreasonable. Therefore, the storage capacities are the local minima.

7. Discussion and application

The three-dimensional rotation neural network is an extension of the Hopfield model, the four-state complex model, the complex phasor model and the Hamilton model. In this paper, the absolute and effective storage capacities of the three-dimensional rotation neural network model are discussed by using the signal-to-noise theory with the adiabatic-like approximation. Some results discussed in the Hopfield model, the complex phasor model and the Hamilton neural network are obtained. Unlike other multistate neural networks, for a fixed neuron state Q, the model allows various combinations of states of rotation angles and axes. Therefore, a novel property of the model is that, for a fixed neuron state Q, the storage capacity varies with different combinations of q_0 and q_1, and the maximum storage capacity can be obtained for a special combination of q_0 and q_1. The storage capacity of the model decreases fast with the increase of the neuron state and approaches zero as the neuron state approaches to infinity.
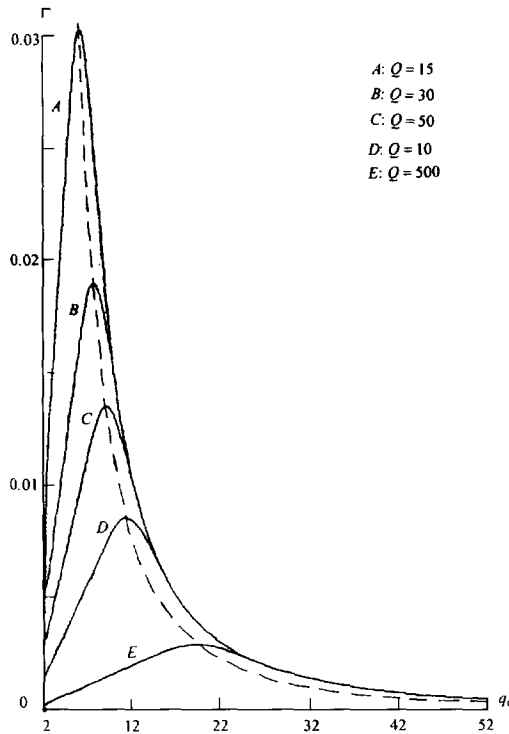
Fig. 8. The effective storage capacity Γ via q_0 with fixed neuron state $Q = 15, 30, 50, 100$ and 500. The maximum storage capacity via Q is given with dashed line.

Due to the four components of the neuron state, the model can be applied to recognize the color patterns that are widely used in computers. The corresponding relationship between the three-basic-color computer code and the three-dimensional rotation neuron code of the color patterns can be set up naturally and simply: The three direction angles can be corresponded to the three basic colors and the rotation angle corresponded to the color saturation degree. For example, the recognition of sixteen-level color pattern with the sixteen-state Hamilton neural network model is discussed in detail in [20].

Acknowledgements

References

[1] I. Kanter, Potts-glass models of neural networks, Phys. Rev. A 37 (1988) 2739.

[2] H. Rieger, Storing an extensive number of gray-toned patterns in a neural network using multistate neurons, J. Phys. A 23 (1990) L1273.

[3] A.J. Noest, Discrete-state phasor neural networks, Phys. Rev. A 38 (1988) 2196.

[4] J. Cook, The mean-field theory of a Q-state neural network model, J. Phys. A 22 (1989) 2057.

[5] J.J. Hopfield, Neural networks and physical systems with emergent collective computational abilities, Proc. Natl Acad. Sci. USA 79 (1982) 2554.

[6] D. Bolle and G.M. Shim, Nonmonotonic behavior of the capacity in Phasor neural networks, Phys. Rev. E 50 (1994) 5043.

[7] J.W. Shuai, Z.X. Chen, R.T. Liu and B.X. Wu, The Hamilton neural network model, Physica A 216 (1995) 20.

[8] J.W. Shuai, Z.X. Chen, R.T. Liu and B.X. Wu, The 2^n-element number neural network model: recognition of the multistate patterns, J. Mod. Opt. 42 (1995) 1179.

[9] C.H. Zhou and L.R. Liu, The complex Hopfield model, Opt. Commun. 103 (1993) 29.

[10] Y. Nakamura, K. Torii and T. Munakata, Neural-network model composed of multidimensional spin neurons, Phys. Rev. E 51 (1995) 1538.

[11] A.J. Noest, Associative memory in sparse phasor neural network, Europhys. Lett. 6 (1988) 469.

[12] G.Y. Sirat, A.D. Maruani and Y. Ichioka, Gray level neural network model, Appl. Opt. 28 (1989) 414.

[13] Z.X. Chen, J.W. Shuai, R.T. Liu and B.X. Wu, The stability of the 2^n-element number neural network models, Physica A 218 (1995) 291.

[14] Z.X. Chen, J.W. Shuai, J.C. Zheng, R.T. Liu and B.X. Wu, The storage capacity of the complex phasor neural network, Physica A 225 (1996) 157.

[15] R.J. Mceliece, E.D. Posner, E.R. Rodemich and S.S. Venkatesh, The capacity of the Hopfield associative memory, IEEE Trans. Inform. Theory 33 (1987) 461.

[16] A.D. Bruce, E.J. Gardner and D.J. Wallace, Dynamics and statistical mechanics of the Hopfield model, J. Phys. A 20 (1987) 2909.

[17] S. Amari and K. Maginu, Statistical neurodynamics of associative memory, Neural Networks 1 (1988) 63.

[18] D.J. Amit, H. Gurfreund and H. Sompolinsky, Storing infinite numbers of patterns in a spin-glass model of neural networks, Phys. Rev. Lett. 55 (1985) 1530.

[19] A.C.C. Coolen and D. Sherrington, Dynamics of fully connected attractor neural networks near saturation, Phys. Rev. Lett. 71 (1993) 3886.

[20] J.W. Shuai, Z.X. Chen, R.T. Liu and B.X. Wu, Hamilton neural network model: recognition of the color patterns, Appl. Opt. 34 (1995) 6764.